A Comparison of Interpolation Methods for Breast Microwave Radar Imaging

Daniel Flores-Tapia, *Member IEEE*, Gabriel Thomas, *Member IEEE,* Stephen Pistorius, *Senior Member IEEE*

Abstract- **In recent years, Breast Microwave Imaging (BMI) has shown its potential as a promising breast cancer detection technique. This imaging technology is based on the electrical characteristic differences that exist between normal and malignant breast tissues at the microwave frequency range. A promising image formation technique for BMI radar based approaches is wavefront reconstruction. In this approach, the image quality and execution time of this image formation technique is strongly affected by the interpolation method that is used. In this paper, a performance study between three popular interpolation techniques, nearest neighbor, linear and cubic splines, for breast microwave radar imaging is presented. The performance of the evaluated techniques was assessed using numeric phantoms obtained from Magnetic Resonance Imaging (MRI) data sets. The results of this study indicate that linear interpolation techniques are the most suitable choices based on their computational cost, and the focal quality and signal to noise of their resulting images.**

I. INTRODUCTION AND MOTIVATION

During the last decade, the use of microwave techniques as a complimentary tool for breast cancer detection has been proposed [1]. The use of microwaves for breast imaging applications was motivated by the dielectric properties differences between healthy and malignant breast tissues [2]. Breast microwave imaging techniques are based on the use of the diffracted and reflected fields produced when a breast structure is irradiated using a microwave waveform to form an image. One of the most promising microwave technologies for breast cancer detection is Breast Microwave Radar Imaging (BMRI). Similar to conventional radar applications, BMRI systems irradiate an electromagnetic waveform into the scan area. The backscattered signals from the different breast structures are then recorded, processed and then displayed so they can be visualized and interpreted.

A common way to collect BMRI is performed along circular scan geometry in order to better suit the geometry of the breast region. As discussed in [3], the reflections from the different breast structures form non-linear signatures. This fact makes difficult to determine the correct dimensions and locations of the different scattering

Daniel Flores-Tapia and Stephen Pistorius are with the Department of Medical Physics, CancerCare Manitoba, Winnipeg, Manitoba, R3E 0V9,Canada,(email:daniel.florestapia,stephen.pistorius@cancercare.mb.ca.

Gabriel Thomas are with the Electrical and Computer Engineering Department, University of Manitoba, Winnipeg, Manitoba, R3T 5V6 Canada (phone: (204) 474-6893, fax: (204) 261-4639, e-mail: thomas@ee.umanitoba.ca).

structures present in the scan area. In order to properly visualize the targets reflections, the collected reflections must be focused [3]. One of the most promising BMRI image formation approaches is wavefront reconstruction. Results presented in [3] show that this reconstruction technique produces images with high Signal to Noise Ratio (SNR) and focal quality values. Wavefront reconstruction techniques perform a series of operation on the frequency domain to form an image of the collected backscattered fields. Due to the fact that most of the BMRI data is acquired and processed using digital equipment, the collected data, $s(t,\theta)$ usually has the form of an evenly sampled discrete space. The sampled version of $s(t,\theta)$, $s(t_l,\theta_n)$ is defined over an LxN grid, where L is the number of time samples, N is the total scan locations in the circular scan pattern and l and n are the sample indexes in the t and θ directions respectively. To be able to visualize the compensated data in a rectangular coordinate system, $s(t_l,\theta_n)$ must the transferred to a rectangular space (x,y).

This is done usually this is done using the following mapping:

$$S_c(\omega_m, \theta_n) = I(k_x^u, k_y^u) \qquad (1)$$

where

$$k_x^u = \omega_m/v \cdot \cos(\theta_n),\ k_y^u = \omega_m/v \cdot \sin(\theta_n) \quad (2)$$

And $S_c(\omega_m, \theta_n)$ is the compensated version of $s(t_l,\theta_n)$ [3], ω_m is the mth frequency component of the irradiated waveform, θ_n is the nth scan location, $m = \{1,2,3,..,L\}$, $n = \{1,2,3,..,N\}$ and v is the average propagation speed of the medium. This mapping process has a nonlinear nature, resulting in the formation of a non-evenly spaced set of frequency points. The spectrum corresponding to this set of frequency locations cannot be processed using conventional Fourier techniques. In order to produce an evenly spaced spectrum, the mapped data must be interpolated.

Results presented on [4] indicate that the use of different interpolation techniques has an impact on the SNR and focal quality of radar images acquired in scenarios where a rotational location shift exists. In this paper, a performance study of three popular interpolation techniques, nearest neighbor, bilinear and cubic spline interpolation, in BMRI scenarios is presented. The SNR, focal quality and computational cost of the evaluated techniques were assessed using numerical phantoms obtained from Magnetic Resonance Imaging (MRI) data sets. This paper is organized as follows. An introduction to interpolation

theory on unevenly sampled spaces and the mathematical basis for the evaluated methods is given in section 2. A comparison between the evaluated interpolation techniques is shown and discussed in section 3. Finally, concluding remarks can be found in section 4.

II. INTERPOLATION OF UNEVENLY SAMPLED SPACES

Consider the ordinate pairs (k_x^u, k_y^u) where $u \in \{1, 2, \dots, q\}$ and $q = L \cdot M$. Due to the nonlinear nature of the mapping functions in (1), the sample spacing in this frequency space is not uniform. Although spectral data of this type can be processed using Fourier techniques that consider non equidistant sampling, the resulting images exhibit reduced spatial resolution and the formation of ringing artifacts. If conventional Fourier techniques are to be used, an interpolation process must be performed to generate an evenly sampled spectrum. This can be accurately done using a triangulation mesh basis.

Consider the points contained in the set $P = \{P_1, P_2, P_3, \dots, P_i, \dots, P_q\}$, where P_i is the ith ordered pair in (k_x^u, k_y^u) and $q = L \cdot M$. A triangulation T is asset of N triples of points (P_i, P_j, P_k), where $i, j, k \in \{1, 2, \dots, q\}$ and (P_i, P_j, P_k) are pairwise distinct such that for each triple, the corresponding points are the vertices of a triangle with the properties that each such triangle contains only those three points of P and those are the vertices, that the intersection of the interiors of any two triangles is empty, and that the unions of those triangles is the complex hull of P[5]. For any set of points, there are almost always several triangulations. To optimize this topological process, a Delaunay triangulation algorithm is often used. This approach optimizes the triangulation process by evaluating the smallest angle in each of the possible triangulations present in the evaluated set [5]. This algorithm is described in detail on [6]. From this point, a wide variety of interpolation basis can be used to generate a function $I(k_x, k_y)$ that defines the behavior of the spectral data contained in (k_x^u, k_y^u) over the evenly sampled frequency space (k_x, k_y).

a) Nearest neighbor interpolation

In the nearest neighbor approximation, the interpolated point Q_i is assigned the value of the closest data point in n-dimensional space. This process yields a piece-wise constant function. In an uneven frequency space, this is interpolation technique is performed by determining the cell within the Voronoi diagram of the frequency space where the Q_i is located. A Voronoi diagram is a set of polytopes generated by partitioning a plane with h points into convex polygons such that each polygon contains exactly one generating point and every point in a given polygon is closer to its generating point than to any other. The Voronoi diagram of a set of points g can be determined by calculating the dual graph of the Delaunay triangulation T
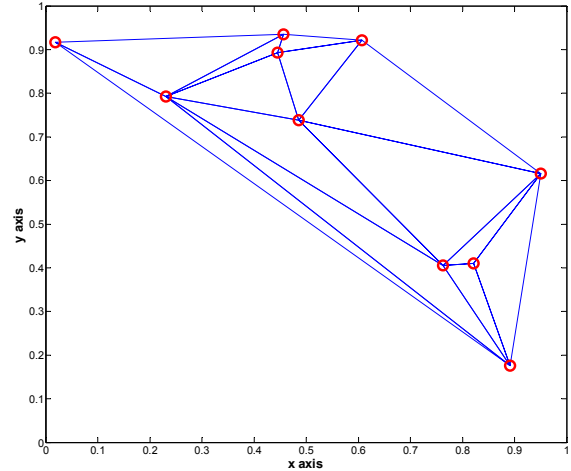
associated with g.

Figure 2. Delaunay triangulation of 10 random data points in the (x,y) plane.

b) Linear interpolation

From elemental analysis, it is known that three distinct non-collinear points in R3 define a plane. Given a triangulation T over P, an interpolating plane can be constructed over each individual triangle in T [5]. Let suppose that we take the triangle $t_{u,v,w}$ formed by P_u, P_v, and P_w. If we write the interpolating plane as:

$$E_{u,v,w}(k_x, k_y) = a + b(k_x - k_x^u) + c(k_y - k_y^u) \quad (3)$$
$$\forall (k_x, k_y) \in t_{u,v,w}$$

Then the interpolation conditions may be written as:

$$\begin{pmatrix} 1 & 0 & 0 \\ 0 & (k_x^v - k_x^u) & (k_y^w - k_y^v) \\ 0 & (k_x^w - k_x^v) & (k_y^w - k_y^v) \end{pmatrix} \begin{pmatrix} a \\ b \\ c \end{pmatrix} = \begin{pmatrix} I(k_x^u, k_y^u) \\ I(k_x^v, k_y^v) \\ I(k_x^w, k_y^w) \end{pmatrix} \quad (4)$$

Then with

$$d = (k_x^v - k_x^u)(k_y^w - k_y^u) - (k_x^w - k_x^u)(k_y^v - k_y^u) \neq 0 \quad (5)$$

The coefficients are given by:

$$a = I(k_x^u, k_y^u) \quad (6)$$
$$b = \frac{1}{d}\Big(\big(I(k_x^v, k_y^v) - I(k_x^u, k_y^u)\big)(k_y^w - k_y^u) - \big(I(k_x^w, k_y^w) - I(k_x^u, k_y^u)\big)(k_y^v - k_y^u)\Big) \quad (7)$$

$$c = \frac{1}{d}\Big(\big(I(k_x^w, k_y^w) - I(k_x^u, k_y^u)\big)(k_x^v - k_x^u) - \big(I(k_x^v, k_y^v) - I(k_x^u, k_y^u)\big)(k_y^w - k_y^u)\Big) \quad (8)$$

By repeating this process all over T, a piece-wise linear function $I_l(k_x, k_y)$ can be determined. From this point, all that is needed is to determine the triangles in which the

interpolation points are located and calculate their values using the corresponding $E_{u,v,w}(k_x, k_y)$ function.

c) Cubic spline interpolation

Splines are piece-wise polynomial functions used as an interpolation basis to model a sampled function so that a set of $n + 1$ data points can be represented by n functions. Cubic splines are the most commonly used due to the fact that this kind of functions minimizes the functional:

$$J(f) = \int_{\varepsilon_1}^{\varepsilon_2} |f''(k)|^2 \qquad (9)$$

over all the Sobolev space $H^2([\varepsilon_1, \varepsilon_2])$. This condition assures that the cubic spline is the smoothest function that can be use to fit a series of data points in the interval $[\varepsilon_1, \varepsilon_2]$ [7]. Define a 1D function $l(k^z)$ defined over a set of values k^z in the k domain, where $i \in \{1, 2, \ldots, Z\}$. The ith segment of a cubic spline function, $C(k)$, is used to interpolate the value of n points in the interval $[k^i, k^{i+1}]$ is defined by:

$$C_i(k) = \alpha_i(k - k^i)^3 + \beta_i(k - k^i)^2 + \gamma_i(k - k^i) + \delta_i \ (10)$$

where:

$$\alpha = \left(C'_{i+1}(k^{i+1}) - C'_i(k^i) \right)/6h_i \qquad (11)$$

$$\beta = C'_i(k^i)/2 \qquad (12)$$

$$\gamma = \frac{\left(l(k^{i+1}) - l(k^i) \right)}{h_i} - \frac{\left(2h_i C'_i(k) - h_i C'_{i+1}(k) \right)}{6} \qquad (13)$$

$$\delta = l(k^i) \qquad (14)$$

where $h_i = k^{i+1} - k^i$. The values of the coefficients are calculated using the iterative approach described in [7]. The adjacent spline segments keep continuity in their curvature and slope at the values defined in k^i, also called knots. Over a triangulated space, every 2D cubic spline segment is defined using 10 coefficients. This poses a problem on any given element of T, due to the fact that only 3 points are available to generate the spline function [5]. To solve this problem, each triangle in T is divided into 3 subtriangles by directing a line from each vortex to the centroid of the triangle. Then, the partial derivatives of at the center, vortexes and bisection points are calculated. Using these values, an iterative procedure similar to the one used for (8) is used to calculate the coefficients of each segment of the 2D cubic spline function $I_C(k_x, k_y)$ over T. A detailed explanation of the algorithm is given in [5]. An example illustrating the results obtained by each interpolation method on a set of randomly generated data points is shown in figure 3.

IV. RESULTS

In order to assess the capabilities of the evaluated methods, two simulated data sets were produced using the radar simulator described in [8]. These data sets were generated using a simulated pattern of 72 scan locations with a 0.4m radius in the *x-y* plane. MRI data sets were used to generate the numeric phantoms. These data sets were obtained from the University of Wisconsin-Madison online phantom repository. The dielectric properties of the breast regions contained in the MRI data sets were determined using the values published in [2]. A Stepped Frequency Continuous Wave (SFCW) was used as the irradiated signal. The SCFW had a bandwidth of 11 GHz with a center frequency of 6.5 GHz. The proposed method was implemented in a desktop PC with a 2.6 GHz Phenom 9950 Quad CPU and 8 GB RAM.
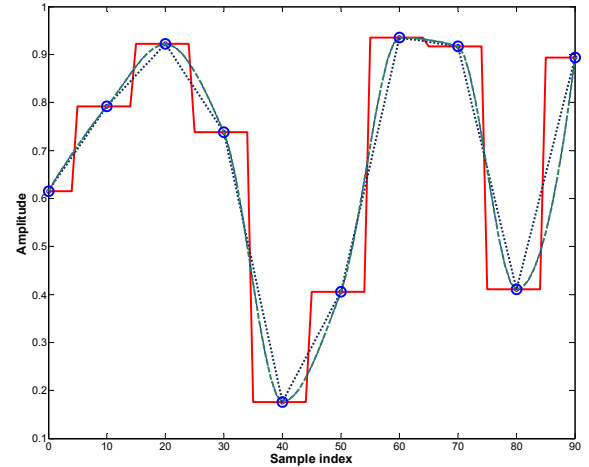

Figure 3. Interpolation functions generated using: Nearest neighbor (thick line), linear (dotted line), and cubic spline interpolation (dashed line).

The evaluated techniques were tested and validated using a MATLAB development environment. The performance of the evaluated methods was quantitatively measured using two metrics, Signal to Noise Ratio (SNR) and conditional entropy, denoted as *H*, [3]. The SNR of the reconstructed images technique was calculated as follows:

$$SNR = 20 \cdot log_{10} \left(\sum_{j=1}^{\alpha} \Gamma_{j,3dB} \Big/ \alpha \Big/ \sigma^w \right) \qquad (15)$$

where $\Gamma_{j,3dB}$ is the magnitude of the 3dB point of the jth scattering source in the image reconstructed by the evaluated algorithm, α is the total number of scatter sources, and σ^w is the standard deviation of the background noise. In this paper, the reflections from the fibroglandular tissue areas were not considered as noise due to the fact that these regions can provide anatomical information for post-reconstruction processing, i.e. image fusion.

The results of an initial experiment using the evaluated techniques can be seen in figure 4. In this experiment, a tumor with a diameter of 5mm was inserted at (-0.02,-0.017) m. In order to have a better visualization of the reconstructed target responses, the surface reflections were removed using the method used by the authors in [3]. The

red circle denotes the location of the removed skin reflections. A second numerical setup and its corresponding reconstructed images are shown in figure 5. For this experiment, a tumor with a diameter of 5mm was inserted at (0.0125,-0.0025) m. Notice the artifact formation on the images generated using the cubic spline approach. The authors believe that the smoothness constraints that inherent to the cubic spline approach are the cause of these artifacts.
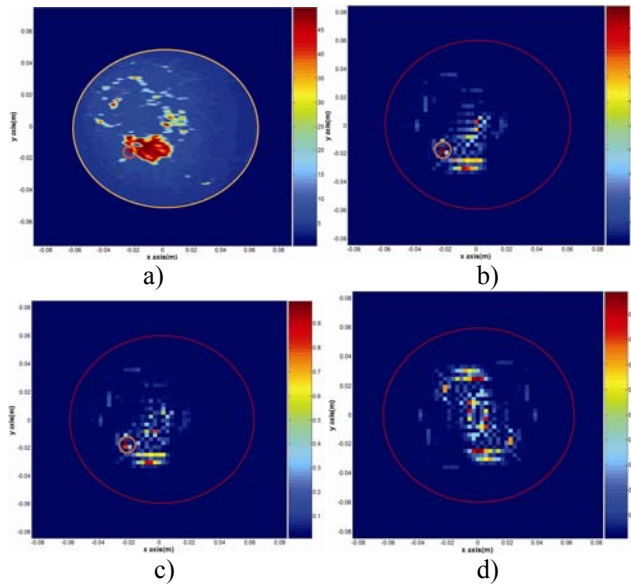

a)   b)

c)   d)

Figure 4. a) MRI model, b) Reconstructed image using linear interpolation, c) Reconstructed image using nearest neighbor interpolation, d) Reconstructed image using cubic spline interpolation. The tumor responses are encircled with an orange contour.
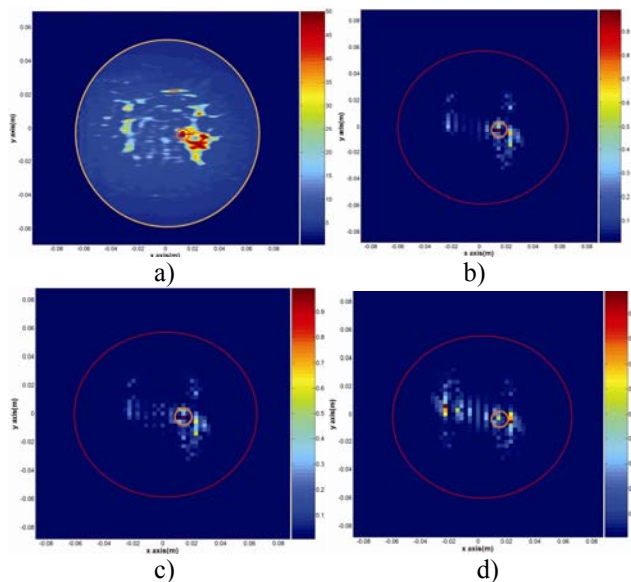

a)   b)

c)   d)

Figure 5. a) MRI model, b) Reconstructed image using linear interpolation, c) Reconstructed image using nearest neighbor interpolation, d) Reconstructed image using cubic spline interpolation. The tumor responses are encircled with an orange contour.

The resulting SNR and conditional entropy values obtained in each experiment are summarized in Table 1. Finally, the computational cost of the proposed technique was evaluated by calculating the average execution time 30 simulated data sets. The average execution time was 31, 35.4 and 240 seconds for the nearest neighbor, linear and cubic spline techniques respectively. The tumor response location error in the images generated using the nearest neighbor and linear interpolation was 5mm.

TABLE I
SNR and Conditional Entropy value comparison in each experiment.

Technique/Experiment		SNR(dB)	H (bits)	Error (mm)
Nearest Neighbor	1	4.93	4.7	5
	2	8.12	1.58	5.5
Linear	1	5.94	4.8	5.1
	2	9.84	1.58	5.6
Cubic	1	2.18	4.86	40
	2	5.81	2	12

V. CONCLUSION

A performance study of three popular interpolation techniques for 2D BMRI reconstruction was presented in this paper. From the results obtained using numerical phantoms, it can be shown that linear interpolation offers the best balance between SNR and focal quality values. The gains in SNR values (20%) are justified by the low computational overhead (10%) compared with nearest neighbor approaches.

REFERENCES

[1]   E.C. Fear, S.C. Hagness, P.M. Meaney, M. Okoniewski, M.A. Stuchly, "Enhancing breast tumor detection with near-field imaging," *IEEE Microwave Magazine*, vol. 3, pp. 48-56, March 2002.

[2]   M. Lazebnik, L. McCartney, D. Popovic, C. B. Watkins, M. J. Lindstrom, J. Harter, S. Sewall, A. Magliocco, J. H. Booske, M. Okoniewski, and S. C. Hagness, "A large-scale study of the ultrawideband microwave dielectric properties of normal breast tissue obtained from reduction surgeries," *Physics in Medicine and Biology,* vol. 52, pp. 2637-2656, April 2007.

[3]   D. Flores-Tapia, G. Thomas and S. Pistorius, "A wavefront reconstruction method for 3D cylindrical subsurface radar imaging," *IEEE Transactions on Image Processing*, vol. 17, pp. 1908-1925, October 2008.

[4]   J. Sok-Son, G. Thomas, and B. C. Flores, *Range-Doppler Radar Imaging and Motion Compensation*, Artech House, Inc. Norwood, MA, USA, February 2001.

[5]   H. Späth, *Two dimensional spline interpolation algorithms*, A K Peters Ltd., Wellesley, MA, USA, 1995.

[6]   C. B. Barber, D. P. Dobkin and H. Huhdanpaa, "The quickhull algorithm for convex hulls," *ACM Transactions on Mathematical Software,* vol. 22, pp. 469-483, December 1996.

[7]   H. Späth, *One dimensional spline interpolation algorithms*, A K Peters Ltd., Wellesley, MA, USA, 1995.

[8]   D. Flores-Tapia, G. Thomas, A. Sabouni, S. Noghanian, S. Pistorius, "Breast tumor microwave simulator based on radar signal model", *2006 IEEE International Symposium on Signal Processing and Information Technology,* vol. 1, pp 17-22, August 2006.